Comparison of low, medium and high fidelity numerical methods for unsteady aerodynamics and nonlinear aeroelasticity

Claudia Fernandez-Escudero, Miguel Gagnon, Eric Laurendeau, Sebastien Prothin, Guilhem Michon, Annie Ross

▶ **To cite this version:**

Claudia Fernandez-Escudero, Miguel Gagnon, Eric Laurendeau, Sebastien Prothin, Guilhem Michon, et al.. Comparison of low, medium and high fidelity numerical methods for unsteady aerodynamics and nonlinear aeroelasticity. Journal of Fluids and Structures, 2019, 91, pp.102744 -. 10.1016/j.jfluidstructs.2019.102744 . hal-03487289v2

HAL Id: hal-03487289
https://hal.science/hal-03487289v2

Submitted on 20 Jul 2022

HAL is a multi-disciplinary open access archive for the deposit and dissemination of scientific research documents, whether they are published or not. The documents may come from teaching and research institutions in France or abroad, or from public or private research centers.

L'archive ouverte pluridisciplinaire **HAL**, est destinée au dépôt et à la diffusion de documents scientifiques de niveau recherche, publiés ou non, émanant des établissements d'enseignement et de recherche français ou étrangers, des laboratoires publics ou privés.

Distributed under a Creative Commons Attribution - NonCommercial 4.0 International License

Version of Record: https://www.sciencedirect.com/science/article/pii/S0889974618307096
Manuscript_5f706d2f069349c44ba51d2f0ec03b7e

Journal of Fluid and Structures. Special Issue: IUTAM Symposium on *Critical flow dynamics involving moving/deformable structures with design applications*, June 18-22, 2018, Santorini, Greece.

Comparison of low, medium and high fidelity numerical methods for unsteady aerodynamics and nonlinear aeroelasticity

Claudia FERNANDEZ-ESCUDERO [(1)], Miguel GAGNON [(2)], Eric LAURENDEAU [(2)], Sebastien PROTHIN [(3)], Guilhem MICHON [(4)], Annie ROSS [(2)]

[(1)] Corresponding Author. ISAE-Supaero, 10 Avenue Edouard Belin, 31400 Toulouse, France/ Polytechnique Montreal, 2900 Edouard Montpetit Blvd, QC H3T 1J4, Montreal, Canada (*Claudia.FERNANDEZ-ESCUDERO@isae-supaero.fr*).
[(2)] Polytechnique Montreal
[(3)] ISAE-Supaero
[(4)] Universite de Toulouse, ICA, CNRS, ISAE-Supaero

Abstract. The unsteady aerodynamic and aeroelastic behaviour of a 2D wing section with and without flap is analysed with Theodorsen theory and Unsteady Vortex Lattice Method (low fidelity), Euler (medium fidelity) and Reynolds-Averaged Navier Stokes (high fidelity) methods. The aeroelastic studies are carried out for linear cases and non-linear structural configurations presenting cubic stiffness and freeplay. The critical flutter speeds as well as the limit cycle oscillations present in the non-linear cases are compared. The methods show good agreement for the cases studied.

Key words: Aeroelasticity; Unsteady Aerodynamics; Flutter; LCO; Non-linear dynamics; Theodorsen; Vortex Lattice Method; Reynolds Averaged Navier Stokes; Euler; Control Surface; Freeplay; Cubic Stiffness

1. Introduction

Aeroelasticity remains today a subject of great interest in aircraft design and analysis. It includes the study of static aeroelastic effects and the analysis of more complex problems which appear when dynamic systems are considered. Moreover, aeroelasticity is often affected by non-linearities which alter the system's response; it is the subject of active research, as can be found in the review paper by (Afonso, 2017). These non-linearities have two different sources: structural elements such as freeplay or cubic stiffness (Breitbach, 1978) can appear alone or simultaneously in any of the degrees of freedom (DOF) of the airfoil (Malher, 2016) and aerodynamic effects which are mainly due to either transonic effects (Jeffrey P. Thomas, 2002) or to dynamic flow separation due to large deflections in wings, known as stall flutter (Malher, 2016). The present paper focuses on the two structural non-linearities mentioned, i.e. freeplay and cubic stiffness.

An important phenomenon encountered in dynamic aeroelasticity is flutter. If there are no sources of non-linearities the system can only experience classic flutter which is defined as self-excited vibration of the structure due to energy extraction of the incident airflow resulting in negative damping and, therefore, a divergent evolution of the amplitude of vibration. One of the causes of this phenomenon is the coalescence of two structural modes: pitch and plunge, which reach the same vibration frequency. Other causes of flutter include transonic effects which cause "dip-flutter", flow separation leading to stall flutter or instabilities in the flow above or below the structure which may result, for example, in buffet or galloping. If the speed becomes higher than the flutter speed, the amplitude of the movement grows

© 2019 published by Elsevier. This manuscript is made available under the CC BY NC user license
https://creativecommons.org/licenses/by-nc/4.0/

exponentially causing structural failure (Bisplinghoff, 1996). A thorough analysis of these aeroelastic problems is presented in (*Progress in Computational Flow-Structure Interaction - Results of the Project UNSI, supported by the European Union 1998 – 2000*, 2003) and in (Lee, Price, & Wong, 1999) which also developed many of the flutter prediction computational methods currently used in the current aeronautics industry.

The presence of non-linearities can change drastically the observed behaviour as other phenomena, such as limit cycle oscillations (LCOs), can appear in the system's response. During a LCO, the vibration reaches a stable amplitude which remains constant unless the wind speed changes. LCOs can be observed in subcritical or in supercritical regime once flutter speed is passed (Thomas, 2002). It has been found that when non-linearities govern the system behaviour, initial conditions may cause the system response to change between two or more possible stable outcomes (Strogatz, 1994). These non-linearities can mainly have two different sources: structural or aerodynamic. Structural non-linearity can be caused by many different elements. Moving parts can have friction or gaps (Y. Zhao, 2004) between them or a nonlinear stiffness, such as a cubic stiffness, (Conner, Tang, Dowell, & Virgin, 1997) (Breitbach, 1978) (Kholodar, 2013), as will be shown further to be our case. Irregular surfaces with, for example, rivets, are also a common source of nonlinearity. These elements are often classified as concentrated (the freeplay) or distributed (the rivets) nonlinearities. The focus of this work will be in concentrated structural non-linearities. As for aerodynamic non-linearities, they are mainly due to either transonic effects (Dowell, Edwards, & Strganac, 2003) or to flow separation due to viscous effects, for instance, large deflections in wings, or perturbing elements on the aircraft (Arévalo, 2008).

The aim of this work is to compare the ability of different numerical methods to capture unstable aerodynamics and aeroelastic behaviour. The aerodynamic forces acting on the airfoil are computed and, together with the equations of motion, enable the calculation of the fluid-structure effects. For the aeroelastic analysis, both the linear and the non-linear cases are studied. In the non-linear 2DOF case, cubic stiffness and freeplay gap are applied in the pitch restoring force whereas only freeplay in the control surface deflection is applied in the 3DOF case. This work follows the work of (Amar, 2017) and includes the use of NLFD (Non-Linear Frequency Domain) for the high fidelity solvers as well as with more accurate time-integration and post-processing techniques.

2. Structural Model

Two configurations are studied regarding the 2D typical wing section: a 2DOF and a 3DOF airfoil. The 2DOF are heave h and pitch α and the 3DOF case refers to an airfoil with an added control surface that can rotate around its elastic axis β. The airfoil is a NACA0012. *Figure 1* presents the degrees of freedom for each case and the main geometrical parameters: b is the semi chord length, ab and cb are the midchord to elastic axis of the profile and of the control surface distance, respectively. Similarly, $x_\alpha b$ and $x_\beta b$ are the centre of gravity to elastic axis distance of the airfoil and of the control surface, respectively.

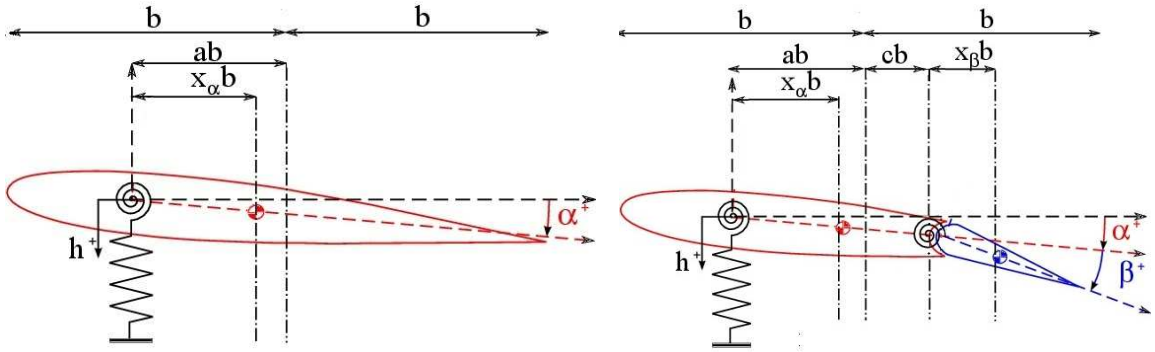

Figure 1. (a) 2DOF and *(b)* 3DOF typical aeroelastic sections. (Amar, 2017)

The dimensionless aeroelastic equation of motion of an airfoil is:

$$M_s\ddot{q} + B_s\dot{q} + (1-\nu)K_s q + \nu f_s(q) = f_a(t) \tag{1a}$$

$$M_s = \begin{bmatrix} 1+\mu_h & x_\propto & x_\beta \\ x_\propto & r_\alpha^2 & r_\beta^2 + (c-a)x_\beta \\ x_\beta & r_\beta^2 + (c-a)x_\beta & r_\beta^2 \end{bmatrix} \tag{1b}$$

$$K_s = \begin{bmatrix} \omega_h^2 & 0 & 0 \\ 0 & r_\alpha^2 & 0 \\ 0 & 0 & r_\beta^2 \end{bmatrix} \tag{1c}$$

$$q = [h/b \quad \propto \quad \beta] \tag{1d}$$

$$f_a = [-L \quad M_\propto \quad M_\beta] \tag{1e}$$

where M_s, B_s and K_s represent respectively the inertial, damping and stiffness matrices, q is a vector containing the degrees of freedom and f_s and f_a are vectors containing respectively the restoring and aerodynamic forces. ν is a switch parameter which has a value of either 1 when the system is non-linear and 0 when the system is linear.

As for the structural damping, matrix B_s is calculated by the method described in (Thomson, 1996) where firstly the eigenvalues of the homogeneous linear system are obtained which enable the calculation of the natural frequencies and the modal mass matrix. Next, the modal mass matrix is obtained and the modal damping matrix is calculated making use of the damping ratios ($\boldsymbol{\zeta}$) obtained experimentally.

In order to solve the fluid structure interaction, a loosely coupled iterative scheme is selected *(see Figure 2)*, whereby the fluid state (W) and structure state (X) are successively updated from iteration n to $n+1$. First, the fluid forces F_a are computed at a given time step and interpolated back onto the structure. The structure state is then computed and the new position, velocity and acceleration ($q, \dot{q}$ and $\ddot{q}$ respectively) are thereafter calculated. The process is then repeated for the next iterative time-step.

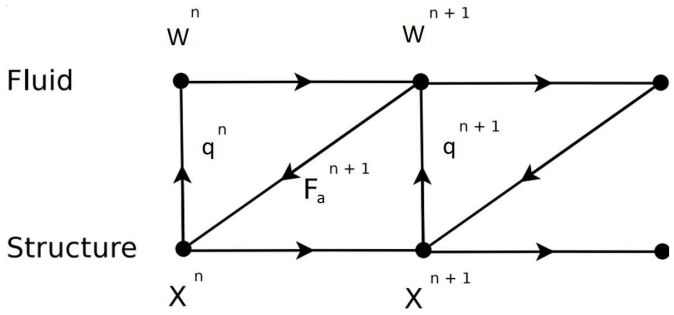

Figure 2: Schema for loosely coupled Fluid-Structure interaction. (Charbel Farhat, 2000)

Non-linearities are introduced in the pitch restoring force in the form of a cubic stiffness and a freeplay gap in the 2DOF (Y. Zhao, 2004) *(see Figure 3).* In the 3DOF case, freeplay is introduced in control surface deflection (Conner et al., 1997). The equations are as follows:

$$f_{s,\alpha} = \begin{cases} r_{\propto}^2 \sum_{k=1}^{n} \eta_{\alpha,k} (\alpha - \alpha_s)^k, & if\ \alpha > \alpha_s \\ r_{\propto}^2 \sum_{k=1}^{n} \eta_{\alpha,k} (\alpha + \alpha_s)^k, & if\ \alpha < -\alpha_s \\ 0, & else \end{cases} \tag{2}$$

$$f_{s,\beta} = \begin{cases} r_{\beta}^2 \sum_{k=1}^{n} \Omega_{\beta,k}^2 (\beta - \beta_s)^k, & if\ \beta > \beta_s \\ r_{\beta}^2 \sum_{k=1}^{n} \Omega_{\beta,k}^2 (\beta + \beta_s)^k, & if\ \beta < -\beta_s \\ 0, & else \end{cases} \tag{3}$$

where α_s and β_s are half of the freeplay angle in pitch and in control surface deflection, $r_{\propto}$ and r_{β} are the reduced radius of gyration defined as $r_{\propto/\beta} = \sqrt{\frac{I_{\propto/\beta}}{mb^2}}$ where m is the mass of the airfoil, $I_{\propto/\beta}$ are the structural inertias, $\eta_{\alpha,k}$ is the ratio between the k^{th} non-linear quadratic stiffness and the linear stiffness and $\Omega_{\beta,k}$ is the reduced uncoupled natural frequency at the k^{th}order.

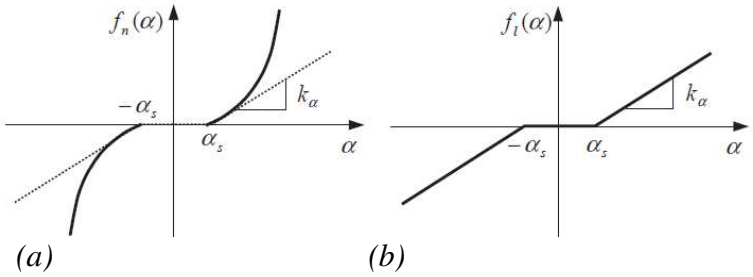

Figure 3. Non-linear pitch stiffness: *(a)* cubic stiffness with freeplay; *(b)* freeplay. (Y. Zhao, 2004)

3. Aerodynamic Models

Different numerical approaches are used to model the aerodynamic forces vector, f_a. These are described at very high level to highlight their respective modelling and computational time differences.

3.1 Theodorsen approach

The Theodorsen approach assumes harmonic motion and is valid for thin profiles with small deflections immersed in linear incompressible and irrotational flows. Its ability to capture LCOs in non-linear cases was demonstrated in (Conner et al., 1997). Contrary to the quasi-stationary force approach, Theodorsen takes into account the effects of the wake on the profile by imposing the impermeability and the Kutta conditions. The vortices shed are assumed to be aligned with the profile resulting in a flat wake. The original formulation is in frequency domain (Theodorsen, 1949) and remains convenient as long as the system is linear. However, for non-linear cases the equations are more easily solved in time domain and the Jones approximation is used (Jones, 1938).

In the case of the frequency domain approach the Theodorsen complex transfer function C(k) is used whereas in time domain, the inverse Fourier transform of this function is used which is called Wagner function (Wagner, 1925). The later function enables the calculation of an augmented variable which is used to obtain the aerodynamic coefficients as shown in (Edwards, 1979).

3.2 UVLM

In the Unsteady Vortex Lattice Method (UVLM), the airfoil and the aileron are discretized into panels and the transport of vortices is accounted for by a shedding wake (Katz & Plotkin., 2001) in the case of the free wake approach. Other options are available for the wake model: a rigid wake which captures the oscillating motion of the wake but, unlike the free wake approach, does not account for the wake roll-up or a linear wake which assumes a flat wake similar to the Theodorsen method *(see figure 4).* Since the results obtained by all three methods, namely free wake, rigid wake and flat wake, were similar for the cases examined in our study, only results with the free wake approach are presented.

Each panel contains a vortex at ¼ of its length and a collocation point at ¾ of the length *(see figure 3).* The vortex points induce a velocity on the rest of the panels and their influence is calculated in the collocation points. The Kutta condition is satisfied by imposing the same vorticity on the shed wake and on the trailing edge panel. The Neumann boundary condition on the airfoil, for the velocity potential, closes the system (Katz & Plotkin., 2001). Some limitations remain, as the thin airfoil and potential flow hypothesis still apply.

The computational implementation of the UVLM code is fully described in (Katz & Plotkin., 2001). The algorithm obtains the vorticity at each point (ɣ) by solving a linear system of equations:

$$AIC * \gamma = RHS \qquad (4)$$

where AIC is the Aerodynamic Influence Coefficients matrix which contains the induced velocities ($v_{j,i}$) calculated as:

$$v_{j,i} = \frac{\gamma_j}{2\pi r_{ij}^2}\begin{Bmatrix} y_i - y_j \\ x_i - x_j \end{Bmatrix} \qquad (5)$$

and RHS is a vector containing the reduced inflow velocity, the reduced airfoil velocity and the position of the airfoil.

Once the vorticities are obtained, the pressure coefficient is calculated using the unsteady Bernoulli equation:

$$C_{p,i} = \frac{\gamma_{i,k}}{\Delta l} * (u_\infty - v_{m,i} + \sum_{l=1}^{k} v_{l,i}) * n_i + \frac{1}{\Delta t}\sum_{m=1}^{i} \gamma_{i,k} - \gamma_{i,k-1} \quad (6)$$

which enables the calculation of the rest of the aerodynamic coefficients.

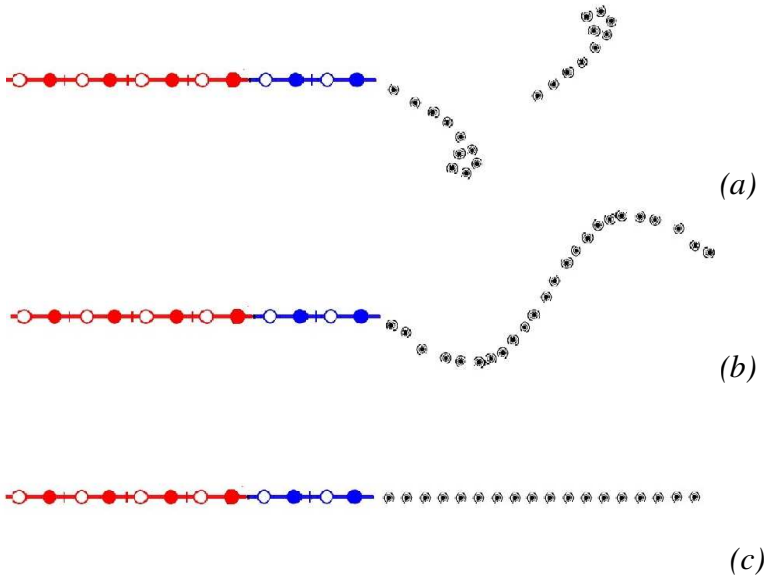

Figure 4. UVLM airfoil discretization. *(a)* free wake *(b)* rigid wake *(c)* flat wake
:airfoil vortex point, :airfoil collocation point, :aileron vortex point, : aileron collocation point, :wake vortex

3.3 Euler and URANS approaches

Euler and Unsteady Reynolds-Averaged Navier Stokes (URANS) solvers compute the aerodynamic forces by solving a set of conservation laws (mass, momentum, energy) at discrete space/time intervals. While the Euler equations are non-linear, they ignore viscous effects. URANS solvers are as Euler solvers, with the addition of the viscous stresses. Turbulence is typically modelled via the eddy viscosity assumption. The aerodynamic solver used is NSCODE (A. T. Levesque, 2015), which uses a cell-centered multiblock structured approach. In this work, we use an implicit LUSGS (Lower-Upper Symmetric Gauss-Seidel) time integration scheme with classical acceleration methods such as multigrid and implicit residual smoothing. For turbulent calculations, the Spalart-Allmaras turbulence model (Spalart & Allmaras, 1992) is selected. Different meshes and different time steps were tested to ensure mesh and time converged solutions. Three levels of O-meshes with 129x129, 257x257 and 513x513 cells were used. The results of the intermediate mesh (257x257) are considered sufficiently converged and are used in the paper. The presented computations use an ALE (Arbitrary Lagrangian Eulerian) formulation. The unsteady Euler model was solved with both DTS (Dual-Time Stepping) (Sicot, Gomar, Dufour, & Dugeai, 2014; Yang, Luo, & Liu, 2005) and NLFD (Non-Linear Frequency Domain) methods (Simpson & Palacios, 2013). For DTS, simulations lasted for 7 complete periods with 500 time steps per period. A convergence analysis was performed with 1000 time steps per period, showing time-step convergence. Regarding NLFD, spectral convergence analysis was carried out with 3, 5 and 6 modes and the results shown correspond to the 3 modes analysis.

3.4 Computation time

Table 1 presents approximate computation time for each of the methods for approximately 10 oscillation cycles (3 initial transient cycles) on a single-core of the Intel 3930K CPU. Note that regarding our cases, the aerodynamic force calculation determines the total computation time since the time taken for the structural equation is comparatively negligible.

Method	Computation Time on Intel 3930K CPU
Theodorsen	~30 seconds
UVLM	~45 minutes
Euler DTS	~8 hours
Euler NLFD (3 modes)	~6 hours
URANS NLFD (3 modes)	~1 day

Table 1. Approximate computation time for each method.

4. Unsteady aerodynamics

As a preliminary step, the potential aerodynamic models are verified for imposed plunge and pitch motions of the 2DOF linear airfoil *(Figures 4 and 5).* The cases chosen are those presented in Murua (Murua, 2012) using UVLM and (Yang, 2006) using Euler respectively. We emphasise that only the aerodynamic forces are considered in this section and not the structure response to these forces.

For each case, the Mach (M) and Reynolds (Re) numbers are given. We observe that the tests are in low subsonic regime where the incompressibility hypothesis is reasonable. The imposed vibration frequency is characterised by the dimensionless reduced frequency $K = \frac{\omega c}{2U_\infty}$ where ω is the oscillating frequency (in rad/s), c is the airfoil chord and U_∞ is the incident flow speed. The dimensionless amplitude of the movement is given by *h/b* in the plunge case. In the pitch case, the airfoil moves around a position referred to as "mean alpha" with amplitude alpha. The low-fidelity methods agree in capturing the aerodynamic coefficient *Cl* at moderate reduced frequency and small oscillations *(Figures 5 and 6). Table 2* shows the aerodynamic coefficients obtained at 4.93° angle of attack by the different methods for the steady flow condition (K=0). One must be careful interpreting the differences. Indeed, airfoil thickness increases lift-curve slopes whereas viscous forces reduce it which explains the differences between Theodorsen and RANS solutions. The Euler solution has more lift than the RANS, and the UVLM lift matches Theodorsen's, as expected.

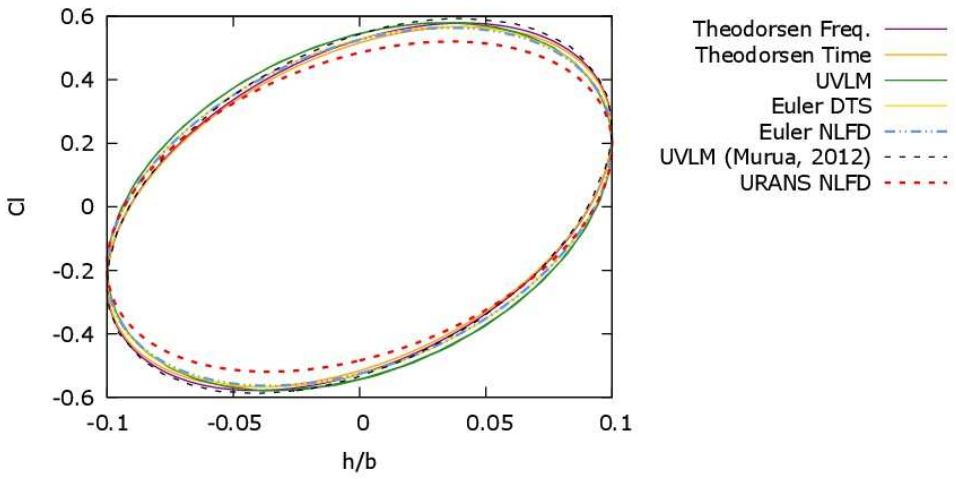

Figure 5. Plunge motion. M=0.1, Re= 1.18M, K=0.75, h/b=0.1

	Theodorsen	UVLM	Euler	URANS
Cl	0.54	0.54	0.63	0.57

Table 2. Steady aerodynamic coefficient. M =0.301, Re=3.91M, K=0, Mean alpha=4.93°

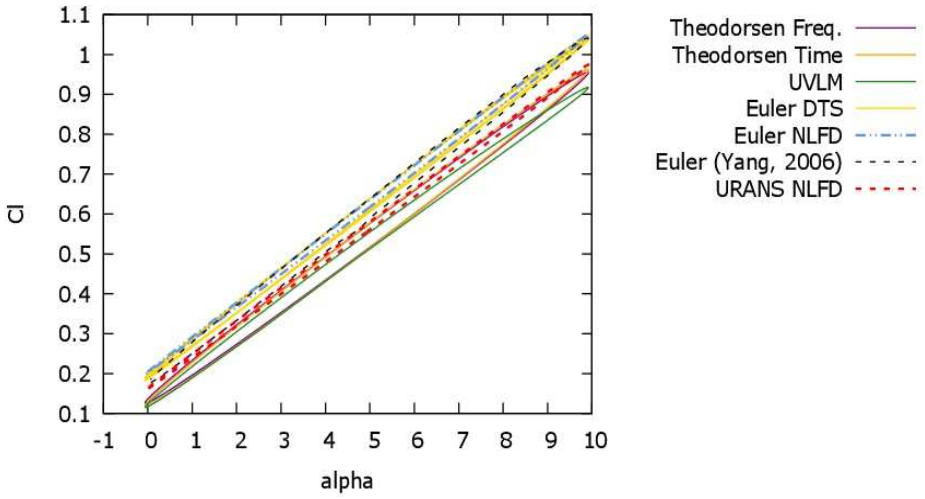

Figure 6. Pitch motion. M=0.301, Re=3.91M, K=0.198, alpha=4.99°, Mean alpha=4.93

5. Linear Aeroelasticity

The flutter analysis is performed on the dimensionless aeroelastic equation of motion of the airfoil *(equation 1)* using the aerodynamic force calculated with the numerical methods already presented. The cases tested are those presented in (Y. Zhao, 2004) using a reduced order flat wake UVLM model and in Conner (Conner et al., 1997) experimentally and numerically for the 2DOF and 3DOF cases respectively. The parameters used are presented in *table 3*. The structural parameters already shown are present, as well as $k = \frac{\rho \pi b^2}{m}$ which is the mass ratio, ζ_h, ζ_α and ζ_β, are the structural damping ratios for each DOF and μ_h is the normalized mass of the support. The natural frequencies of each DOF are represented by ω_h, ω_α and ω_β. $\eta_{\alpha,k}$ is the cubic stiffness and freeplay parameters will be used further on for the nonlinear cases.

Due to the fact that UVLM is in time domain, an extra step is required in order to obtain the results presented. A Fast-Fourier Transform is used to obtain frequency content of the time domain solutions. FFT does not allow the damping to be calculated so a combination of curve fitting and logarithmic decrement techniques are used to capture the damping shown in *Figures 8 and 10.* In these graphs, although there could be as many damping branches as DOFs, only the branch which becomes negative at the flutter point is included for clarity.

	2DOF	3DOF
k	1/100	0.03984
a	-0.5	-0.5
c	n/a	0.5
x_α	0.25	0.434

x_β	n/a	0.01996
$r_\propto$	0.5	0.7321
r_β	n/a	0.11397
ω_h/ω_α	0.2	0.8078
$\omega_\beta/\omega_\alpha$	n/a	2.0746
$\zeta_\propto$	0	0.01626
ζ_h	0	0.0115
ζ_β	n/a	0.0113
freeplay	0.5° (∝)	2.12° (β)
$\eta_{\alpha,k}$	3	0
μ_h	0	1.163627

Table 3. Values of parameters for test cases.

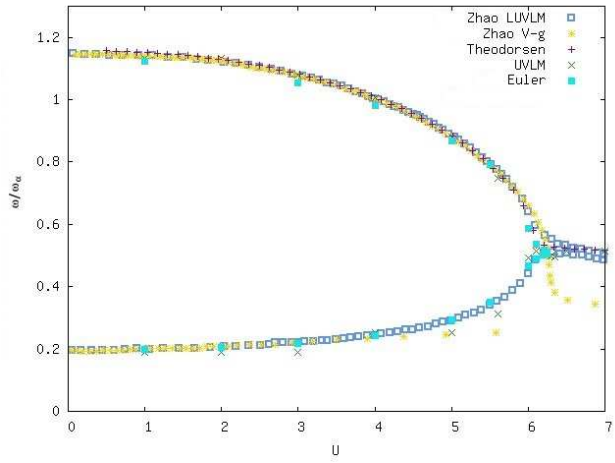

Figure 7. Dimensionless oscillation frequency against dimensionless wind speed for 2DOF linear case.

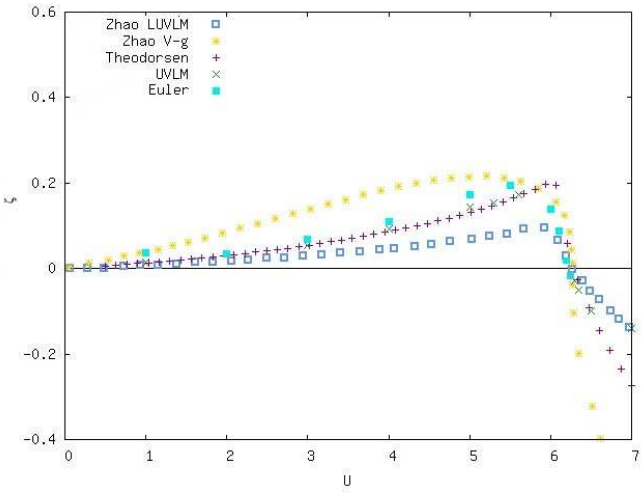

Figure 8. Damping against dimensionless wind speed for the 2DOF linear case.

	Theodorsen	UVLM	Euler	Zhao V-g	Zhao LUVLM
Uf	6.29	6.27	6.29	6.29	6.29

Table 4. Comparison of dimensionless flutter velocities for the 2DOF linear case.

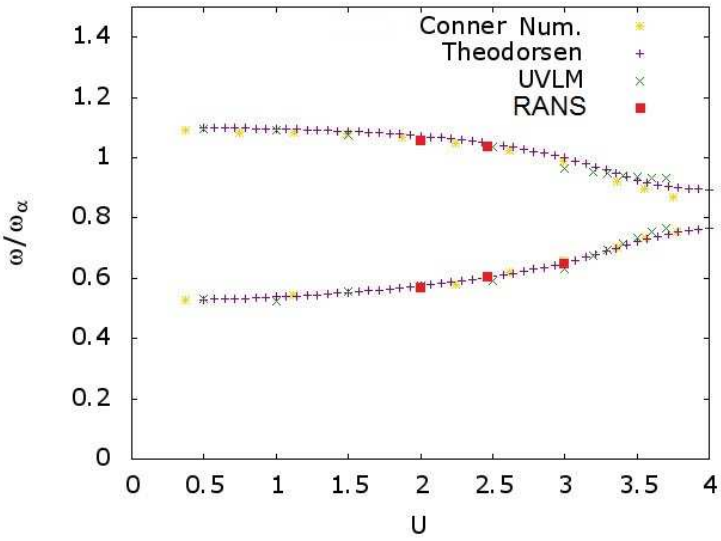

Figure 9. Dimensionless oscillation frequency against dimensionless wind speed for 3DOF linear case.

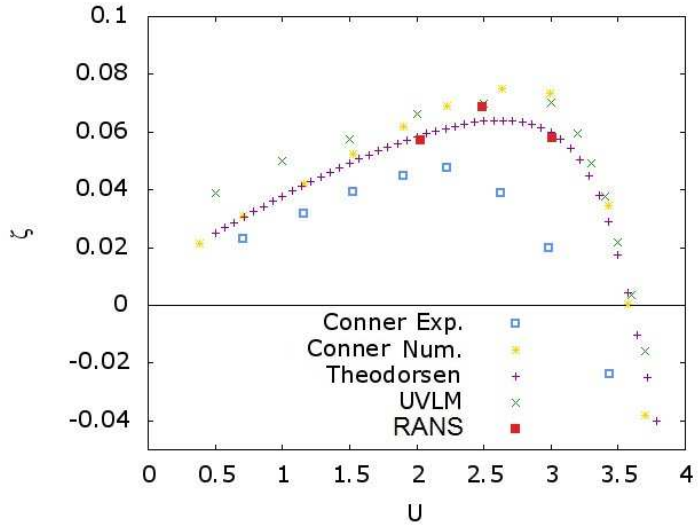

Figure 10. Damping against dimensionless wind speed for the 3DOF linear case.

	Theodorsen	UVLM	Conner Theo	Conner Exp.
Uf	3.57	3.61	3.57	3.08

Table 5. Comparison of linear flutter velocities for the 3DOF linear case.

Figures 7 to *10* show good agreement between Theodorsen, UVLM and Euler or RANS in capturing linear aeroelastic behaviour. These results are compared with (Y. Zhao, 2004) for 2DOF and (Conner et al., 1997) for 3DOF. The values of the flutter speed are obtained, observed as the wind speed at which the damping ratio changes sign in the damping diagrams, and provided in *table 4* for 2DOF and in *table 5* for 3DOF cases. In these cases, a modal coalescence in the frequency diagrams can be observed at a close wind speed. Figures 8 and

10 show reasonably good agreement for the methods presented for all wind speeds but it is seen that the approaches become closer to each other as the system is in the close vicinity to flutter as the system goes from being damped to undamped. This important change of behaviour is thought to be more simply captured than the exact values of positive damping which are not obtained as directly as the modal frequencies for time domain methods and have to be extracted by different means which may give rise to a certain level of uncertainty.

6. Non-Linear Aeroelasticity

For non-linear analysis, the same parameters shown in *table 3* are used but now include the following parametres: *freeplay,* $\eta_{\alpha,k}$ *(the non-linear stiffness power)* and μ_h. Regarding the nonlinear restoring forces, cubic and freeplay non-linearities are introduced in the pitch DOF for the 2DOF case *(figure 11),* and freeplay is introduced in the aileron deflection for the 3DOF case *(figure 12).* The rest of restoring forces in the structural models are kept linear. As for the initial conditions, the 2DOF case *(figure 11)* is started with an initial α of 3° and the 3DOF case *(figure 12)* is started with an initial β of 2,12° similar to the literature cases chosen as due to the nonlinear characteristics of the system, LCO amplitude is dependent on initial conditions.

Below the linear flutter speed, *Uf*, both Theodorsen and UVLM succeeded in capturing the subcritical LCO and were compared with (Y. Zhao, 2004), who used a reduced order linear wake UVLM model named LUVLM, in the 2DOF case. Figure 11 presents dα/dt and dh/dt against α and h respectively for different dimensionless speeds.

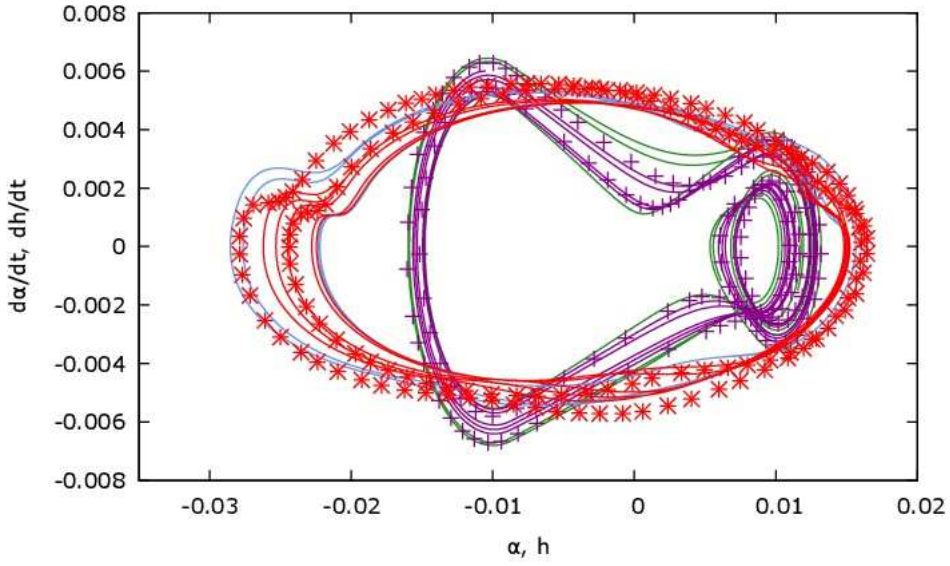
0.008
0.006
0.004
0.002
0
-0.002
-0.004
-0.006
-0.008
dα/dt, dh/dt
-0.03
-0.02
-0.01
0
0.01
0.02
α, h

a)

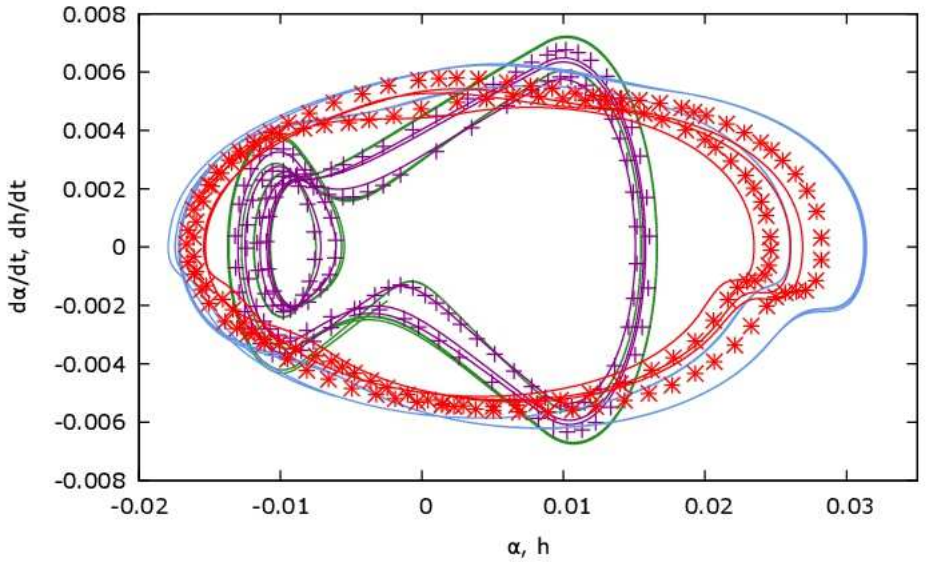
0.008
0.006
0.004
0.002
0
-0.002
-0.004
-0.006
-0.008
dα/dt, dh/dt
-0.02
-0.01
0
0.01
0.02
0.03
α, h

b)

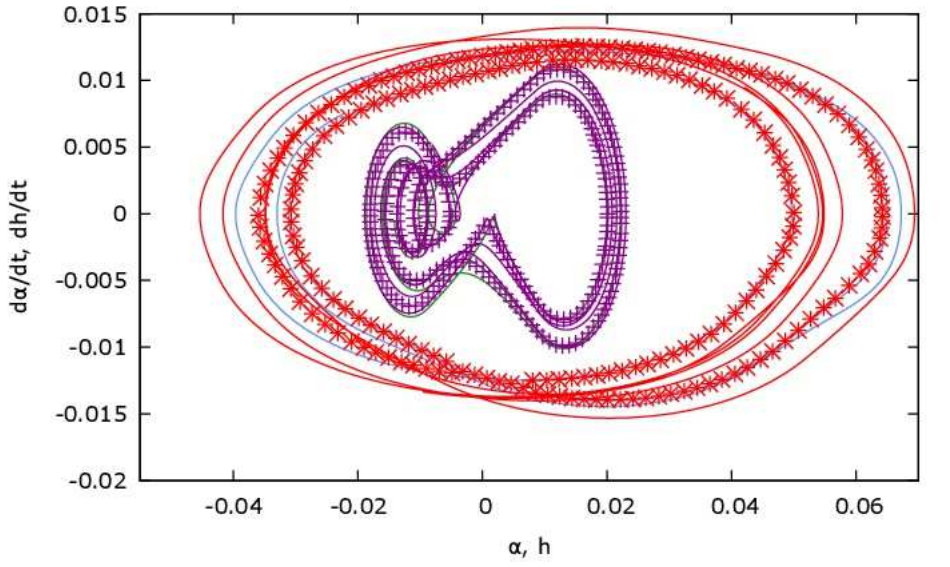
0.015
0.01
0.005
0
-0.005
-0.01
-0.015
-0.02
dα/dt, dh/dt
-0.04
-0.02
0
0.02
0.04
0.06
α, h

c)

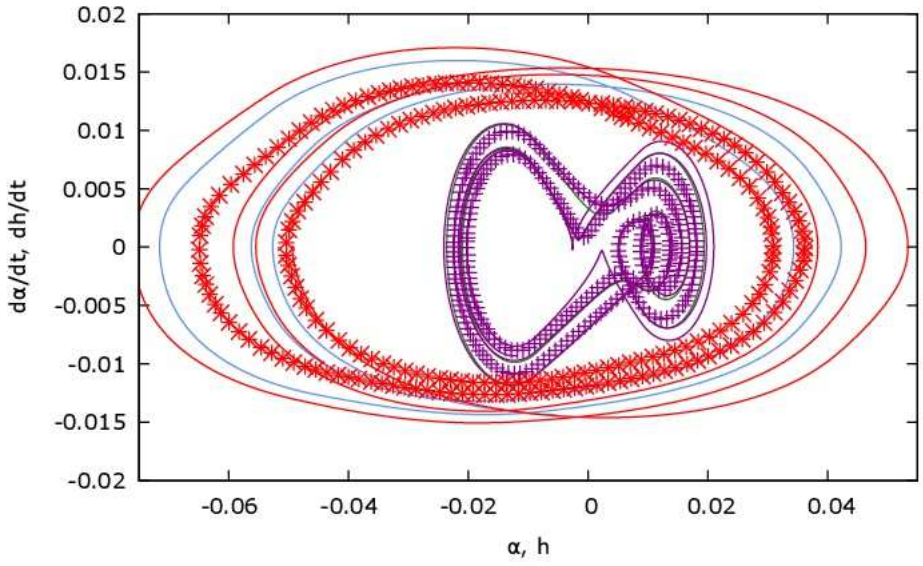
0.02
0.015
0.01
0.005
0
-0.005
-0.01
-0.015
-0.02
dα/dt, dh/dt
-0.06
-0.04
-0.02
0
0.02
0.04
α, h

d)

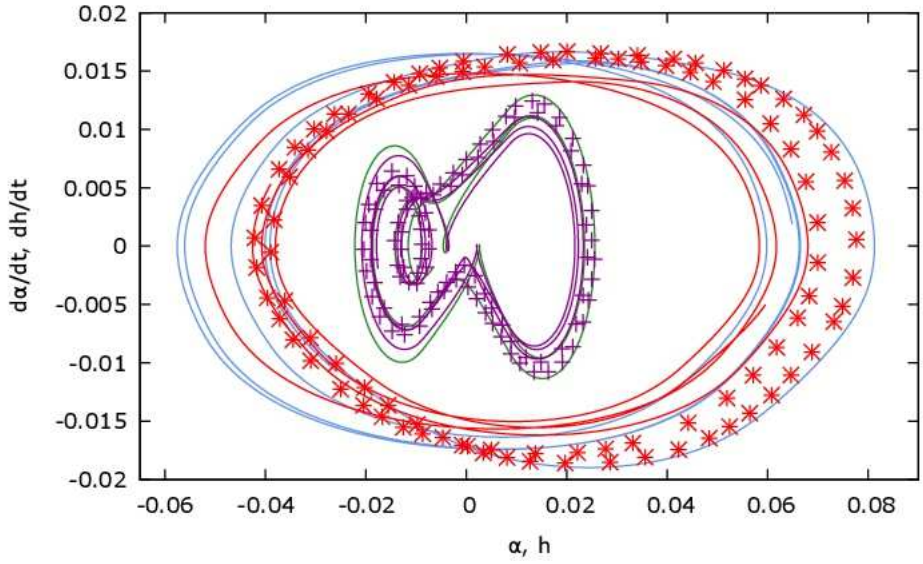
0.02
0.015
0.01
0.005
0
-0.005
-0.01
-0.015
-0.02
dα/dt, dh/dt
-0.06
-0.04
-0.02
0
0.02
0.04
0.06
0.08
α, h

e)

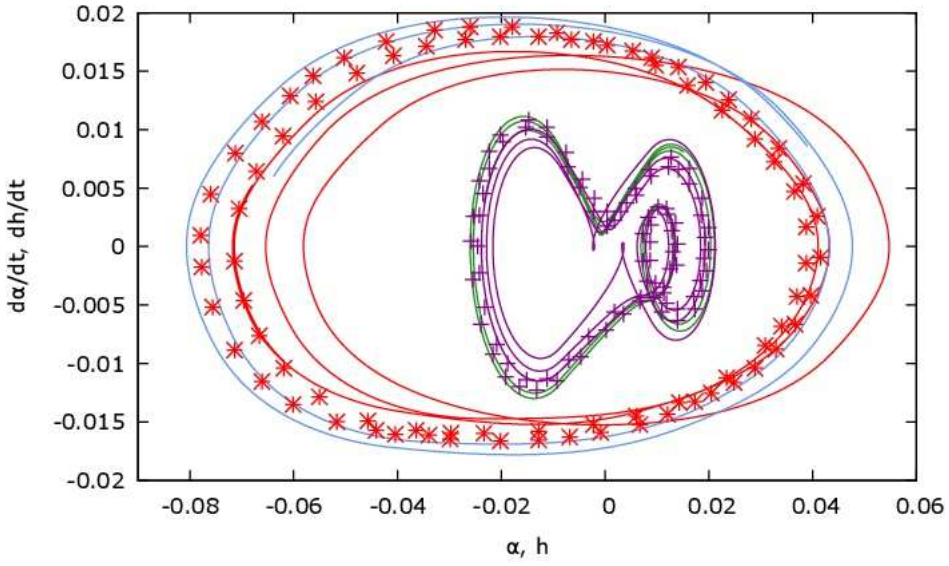
0.02
0.015
0.01
0.005
0
-0.005
-0.01
-0.015
-0.02
dα/dt, dh/dt
-0.08
-0.06
-0.04
-0.02
0
0.02
0.04
0.06
α, h

f)

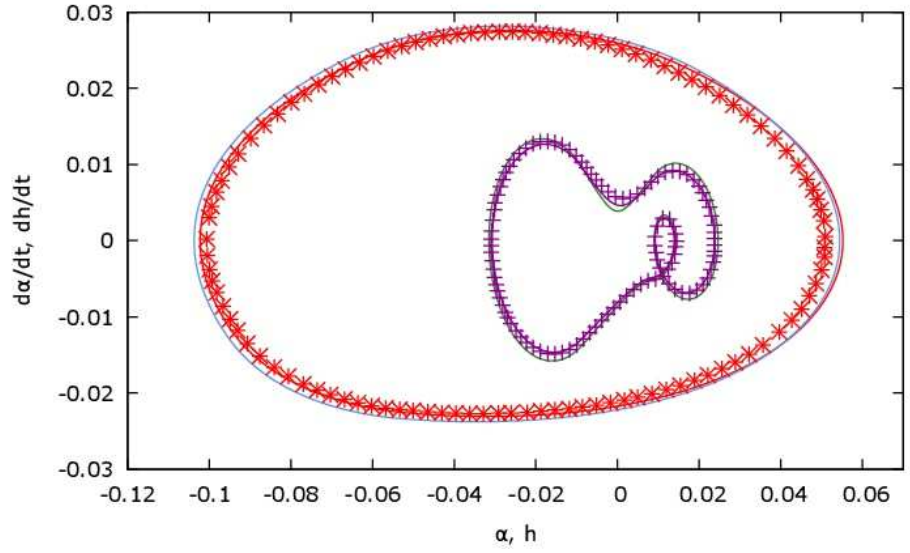
0.03
0.02
0.01
0
-0.01
-0.02
-0.03
dα/dt, dh/dt
-0.12
-0.1
-0.08
-0.06
-0.04
-0.02
0
0.02
0.04
0.06
α, h

g)

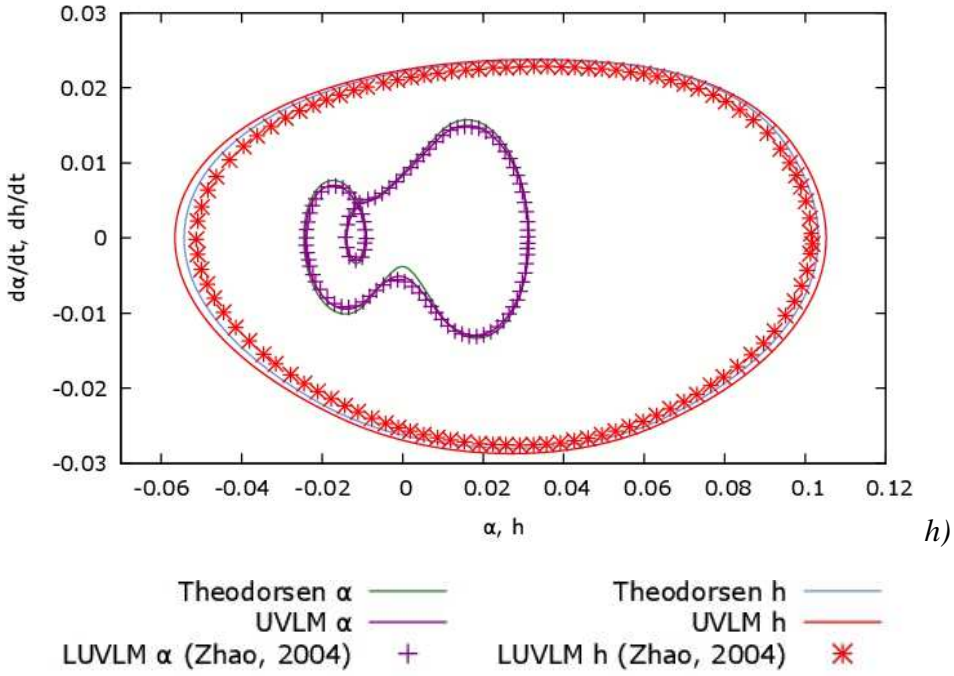

h)

a) **U :** Theo. : 1.850, UVLM : 1.800, Zhao LUVLM : 1.900
b) **U :** Theo. : 2.007, UVLM : 1.860, Zhao LUVLM : 1.912
c) **U :** Theo. : 2.925, UVLM : 2.990, Zhao LUVLM : 2.931
d) **U :** Theo. : 3.140, UVLM : 3.120, Zhao LUVLM : 2.944
e) **U :** Theo. : 3.420, UVLM : 3.140, Zhao LUVLM : 3.453
f) **U :** Theo. : 3.520, UVLM : 3.150, Zhao LUVLM : 3.466
g) **U :** Theo. : 4.160, UVLM : 4.000, Zhao LUVLM : 4.076
h) **U :** Theo. : 4.150, UVLM : 4.010, Zhao LUVLM : 4.089

Figure 11. Change of phase trajectory of subcritical LCO for 2DOF airfoil.

Both the Theodorsen and the UVLM codes have captured a subcritical LCO with four different double symmetric changes of trajectory *(Figure 11),* in agreement with Zhao's work. The authors believe that some of the observed deviations between the presented intermediate figures may be linked to the difficulty experienced in identifying the matching wind speed corresponding to an exact given LCO amplitude due to the fact that the LCO trajectories have a high level of variation as the wind speed increases. It is observed that the α trajectory is closer in all methods than the h trajectory.

For the 3DOF analysis, the literature cases chosen are those presented by (Conner et al., 1997), who also presented experimental data, and (Kholodar, 2013), who used a Doublet Lattice Method (DLM) as well as Theodorsen approach, respectively.

For the 3 DOF non-linear case, the root mean square (RMS) of each DOF's amplitude is calculated and divided by the freeplay gap to compare the results to those obtained by Kholodar (Kholodar, 2013). *Figure 12* shows the results as a function of speed divided by the linear flutter speed where: $(h, \alpha, \beta) = \frac{RMS(h,\alpha,\beta)}{2\beta_s}$.

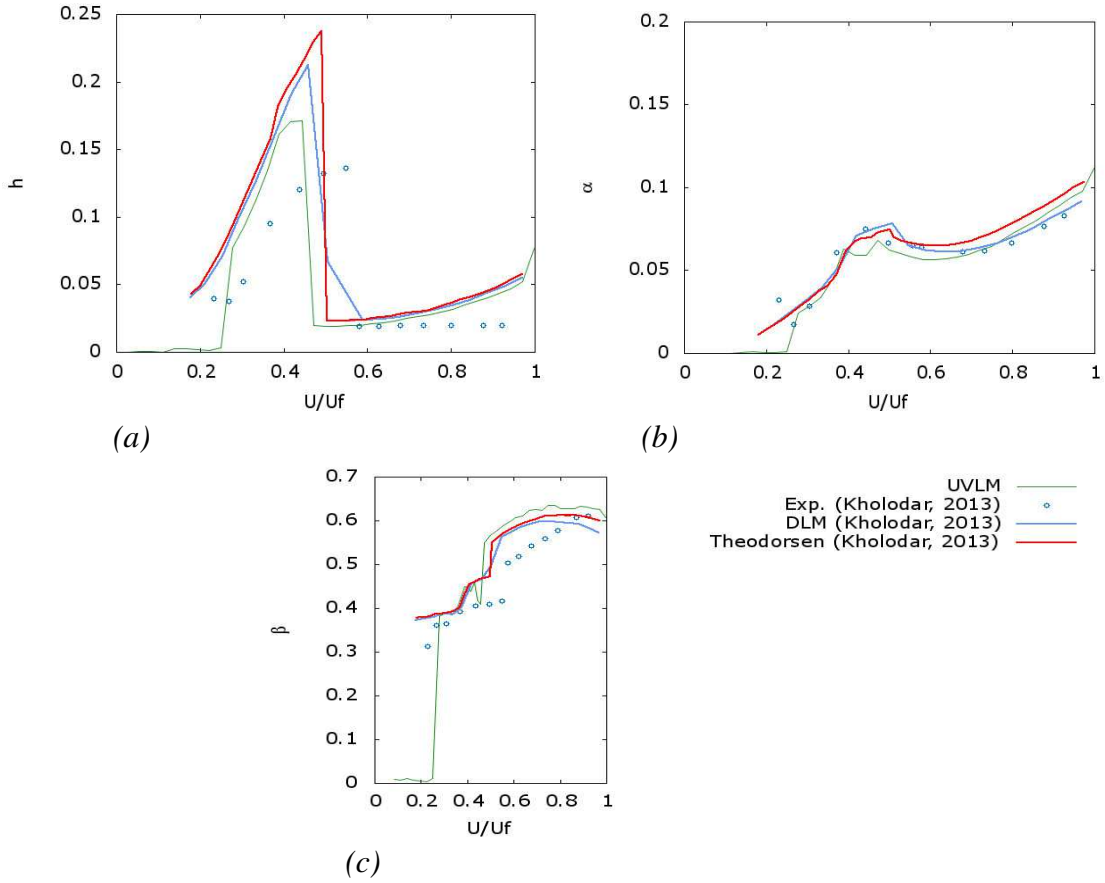

Figure 12. RMS amplitudes as a function of speed over linear flutter speed for *(a)* plunge DOF, *(b)* pitch DOF and *(c)* control surface deflection.

The subcritical LCOs present in the 3DOF system including freeplay are captured as observed in *Figure 12*. For each DOF, motion amplitude varies as linear flutter speed fraction increases. Pitch angle and aileron deflection angle both increase with flow velocity with different rates, as shown by all models. The heaving amplitude increases and then drops to lower amplitude LCO before increasing again as the velocity approaches linear flutter speed.

7. Conclusion

In this work, four methods are used to analyse unsteady aerodynamics and aeroelasticity of a 2D typical wing section: Theodorsen, UVLM, Euler and URANS. The structural models are presented, followed by a brief description of the aerodynamic methods that highlights their differences. Once a mesh/time step validation is carried out to ensure numerical convergence, a pure aerodynamic comparison is performed, showing the agreement between the unsteady aerodynamics low fidelity results and those obtained via Euler (medium fidelity) and URANS (high fidelity) approaches.

Regarding the aeroelastic analysis, the linear flutter speed is identified for a 2DOF and a 3DOF typical section. Non-linearities through freeplay and cubic stiffness in the pitching DOF for the 2DOF case and aileron freeplay for the 3DOF are added to the system to evaluate

its response. Both Theodorsen and UVLM are able to capture subcritical LCOs similar to those identified in the literature.

The computational times of Theodorsen and UVLM are lower by several orders of magnitude than those of URANS or even Euler method. It is concluded that for the cases presented, the low-fidelity methods are capable of capturing the same complex phenomena than for medium or high fidelity methods, at much reduced computational times.

Acknowledgements

The authors would like to acknowledge the Natural Sciences and Engineering Research Council of Canada and ISAE-Supaero for the funding. The work benefited from the advices of Simon Bourgault-Côté and Matthieu Parenteau regarding the software NSCODE and UVLM, respectively.

References

Afonso, F., Vale, J., Oliveira, E., Lau, F., Suleman, A. (2017). A review on non-linear aeroelasticity of high aspect-ratio wings. Progress in Aerospace Sciences. 89. 10.1016/j.paerosci.2016.12.004.

Amar, L. (2017). *Nonlinear passive control of an aeroelastic airfoil, simulations and Experimentations.* PhD Thesis. Toulouse University and Polytechnique Montréal.

Arévalo, F. (2008). *Aeroelasticidad de una aeronave en presencia de nolinealidades estructurales concentradas.* Universidad Politécnica de Madrid. Escuela Técnica Superior de Ingenieros Aeronauticos Madrid.

Bisplinghoff, R. L., Ashley, H., Halfman, R. L. (1996). Aeroelasticity. New York: Dover Publications.

Breitbach, E. (1978) Effects of structural non-linearities on aircraft vibration and flutter. Technical report, DTIC Document.

Charbel Farhat, M. L. (2000). Improved staggered algorithms for the serial and parallel solution of three-dimensional non linear transient aeroelastic problems. *Computer Methods in Applied Mechanics and Engineering*.182. 499-515. 10.1016/S0045-7825(99)00206-6.

Conner, M. D., Tang, D. M., Dowell, E. H., & Virgin, L. N. (1997). Nonlinear behavior of a typical airfoil section with control surface freeplay: a numerical and experimental study. *Journal of Fluids and Structures*. 11. 89-109. 10.1006/jfls.1996.0068.

Dowell, E., Edwards, J., & Strganac, T. (2003). Nonlinear Aeroelasticity. *Journal of Aircraft, 40*(5).

Edwards, J. W. (1979). Unsteady aerodynamic modeling for arbiitrary motions. *AIAA Journal, 17*(4), 365-374.

Farhat, C., Lesoinne, M. (2000). Improved staggered algorithms for the serial and parallel solution of three-dimensional non linear transient aeroelastic problems. Computer Methods in Applied Mechanics and Engineering. 182. 499-515. 10.1016/S0045-7825(99)00206-6.

Jeffrey P. Thomas, E. H. D., Kenneth C.Hall. (2002). Nonlinear Inviscid Aerodynamic Effects on Transonic Divergence, Flutter and Limit-Cycle Oscillations. *AIAA Journal*.

Jones, R. T. (1938). Operational treatment of the nonuniform-lift theory in airplane dynamics. *Technical Notes National Advisory Committee for Aeronautics, 667*.

Katz, J., & Plotkin., A. (2001). Low-Speed Aerodynamics. *Cambridge University Press*.

Kholodar, B. D. (2013). Nature of Freeplay-Induced Aeroelastic Oscillations. *Journal of Aircraft*.

Lee, B. H. K., Price, S. J., & Wong, Y. S. (1999). Nonlinear aeroelastic analysis of airfoils: bifurcation and chaos. *Progress in Aerospace Sciences, 35*(3), 205-334.

Levesque, A. P., Deloze, T., Laurendeau, E. (2015). An overset grid 2D/Infinite swept wing URANS solver using Recursive Cartesian Virtual Grid method. *AAIA*.

Malher, A. (2016). *Amortisseurs passifs non linneaires pour le contrôle de l'instabilité de flottement.* Université de Paris-Saclay, France.

Murua, J. (2012). *Flexible aircraft dynamics with a geometrically-nonlinear description of the unsteady aerodynamics'.* Imperial College

Progress in Computational Flow-Structure Interaction - Results of the Project UNSI, supported by the European Union 1998 – 2000. (2003). (1 ed.): Springer-Verlag Berlin Heidelberg.

Sicot, F., Gomar, A., Dufour, G., & Dugeai, A. (2014). Time-Domain Harmonic Balance Method for Turbomachinery Aeroelasticy. *AIAA Journal, 52*(1), 62-71. doi:10.2514/1.J051848

Simpson, R. J. S., & Palacios, R. (2013). Numerical aspects of nonlinear flexible aircraft flight dynamics modeling. *AIAA*.

Spalart, P. R., & Allmaras, S. R. (1992). A one-equation turbulence model for aerodynamic flows. *30th Aerospace Sciences Meeting and Exhibit Reno,NV,U.S.A.*

Strogatz, S. H. (1994). Nonlinear Dynamics and Chaos with application in physics, biology, chemistry and engineering: Addison-Wesley Publishing Company.

Theodorsen, T. (1949). General theory of aerodynamic instability and mechanism of flutter. . *National Advisory Committee for Aeronautics, 496*.

Thomson, W. (1996). Theory of vibration with applications. *CRC Press*.

Wagner, H. (1925). Über die Entstehung des dynamischer Auftriebes von Tragflügeln. *Z. angew. Math. u. Mech., 5*, 17-35.

Y. Zhao, H. H. (2004). Aeroelastic analysis of a non-linear airfoil based on unsteady vortex lattice model. *Journal of Sound and Vibration*.

Yang, S., Luo, S., & Liu, F. (2005). Computation of the Flows over Flapping Airfoil by the Euler Equations. *AIAA*.